ISSN (Print) : 2320 – 3765

ISSN (Online): 2278 – 8875

International Journal of Advanced Research in Electrical, Electronics and Instrumentation Engineering

(An ISO 3297: 2007 Certified Organization)

Vol. 6, Issue 7, July 2017

Morphology and Optical Properties of SiO_2 Embedded in Porous Alumina Matrix (Al_2O_3) Deposited on Transparent Polypropylene (TPP) Leaf: For Reflective Surfaces

Mondher G[*1,2], Ouartani R[1], Ezzaouia H[1]

[1]Laboratory of Semiconductors, Nanostructures and Advanced Technology (LSNTA), Center for Research and Technology Energy, Tourist Route Soliman, BP 95, 2050 Hammam-Lif, Tunisia

[2]Higher Institute of Sciences and Technologies of the Environment borj cedria tunis Tourist Route Soliman, BP 95, 2050 Hammam-Lif, Tunisia

Abstract: In this work, Silicon oxide (SiO_2) is deposited in a porous alumina matrix (PAM) on transparent polypropylene (TPP) leaf, by a radio frequency plasma enhanced chemical vapor deposition PECVD method. The morphological and microstructural property of (SiO_2/PAM/TPP) structure is investigated by TEM, EDX, XRD technique and Raman spectroscopy. Crystallization of the amorphous SiO_2/PAM/TPP is obtained after deposition at was 650°C at different deposition time ranging from 20 to 60 min. The effect of deposition on the optical properties of SiO_2/PAM/TPP structure was studied by Spectroscopic Ellipsometry (SE) in the spectral range 0.3-0.8 µm. The Ellipsometric analysis demonstrated the formation of mixture layers with SiO_2 diffused in porous alumina barrier layer different deposition time. The optical constants, thickness and the composition of each film have been estimated from the SE data using Bruggeman effective medium approximation. PL spectroscopy was used to investigate the band gap energy of SiO_2/PAM, the origin of emission PL spectra as well as the observed red-shift have been discussed, this observation has been confirmed with reflectivity measurements. As a consequence the reflectivity reaches 99% when SiO_2/PAM/TPP films obtained were SiO_2 deposed at 50 min.

Keywords: Porous alumina matrix; Silicon oxide SiO_2; Transparent polypropylene leaf; Ellipsometry; Photoluminescence; Reflectivity measurements

I. INTRODUCTION

In recent years, structured nanomaterials have attracted considerable attention owing to their interest in potential applications for various fields including optoelectronic nanodevices, and solar panels. Moreover, Silicon oxide (SiO_2) constitutes the basis of microelectronics components. Silicon is an interesting semiconductor because of its excellent opto-electronic properties. Nanoscale structures such as a nanocrystal, quantum dots, quantum wires, nanopillars, are particularly attractive to many applications in nanodevices [1-4]. In this context, many research activities have been particularly devoted to the synthesis and characterization of Silicon oxide (SiO_2). Porous alumina matrix (PAM) has long been used in optical reflector applications. Kennedy et al. [5] have made some advances on aluminum mirrors protected with Al_2O_3 using various substrates. The approach of this work is to elaborate new reflector materials based on SiO_2/PAM/TPP that shows high reflectance compared to that exhibited by conventional Al_2O_3 foil, The most important, this new reflector is very practical, easy to maneuver, low cost, does not absorb water, has a shiny appearance, and is temperature resistant to 160°C. There recently has been a renewed interest in the proper ties of sputtered films for optical applications. SiO_2/PAM/TPP has several undesirable characteristics for reflective applications, including low hardness, no true endurance limit, and rough surface topography relative to porous alumina films [6], As a result, SiO_2/PAM/TPP is rarely used in this form. Fortunately, alumina matrix (PAM) responds extremely well to strengthening deposits Silicon dioxide SiO_2, this can be explained by the nano-mini pore formed in the matrix of the pore of alumina, as function of anodization [7]. This matrix, porous anodic alumina (PAM) layer represents a good candidate to integration SiO2 and oxygen diffusion in the mini-pores having different sizes and shapes. Indeed, PAM/TPP templates characterized by ordered nano-pores structure have recently attracted a vast amount of research attention due to their suitability to deposit different nano-materials, their attractive dielectric, optical properties and their potential applications in medical treatments, magnetic, electronic, optoelectronic and photovoltaic conversion nano-devices [8-21]. Several investigations on the origin and mechanism of light emission of SiO2 have been carried out by Photoluminescence (PL) studies and theoretical models such as the surface state model [22], the defects at the interface of Si/SiO2 [23], and the pure quantum size effect [24-26].

This research aims to study the effects of the deposition time on the morphology and optical properties of SiO_2 in PAM/TPP. XRD and Raman spectroscopy are used to provide information about the crystalline quality. Spectroscopic ellipsometry is an effective

ISSN (Print) : 2320 – 3765

ISSN (Online): 2278 – 8875

International Journal of Advanced Research in Electrical, Electronics and Instrumentation Engineering

(An ISO 3297: 2007 Certified Organization)

Vol. 6, Issue 7, July 2017

technique used for the characterization of layer SiO_2/PAM/TPP thin films. In this paper, SE is used to determine the composition and the optical constants of SiO_2/PAM/TPP thin films during different deposition times. All these studies lead us to clearly identify our new flexible reflector, based through SiO_2/PAM/TPP, which can be used as optical fiber at low cost of production, and high yield.

II. CHARACTERISATION

The crystallographic structure of the annealed SiO_2/PAM/TPP films was carried out by XRD technique using a Bruker D8 advance X-ray diffractometer with CuKα radiation (λCuKα = 0.15406 nm) operated at a high current and tension of 40 mA and 40 kV, respectively. The surface morphology of the films was examined by transmission electron (TEM) and atomic force and microscopies (AFM). The AFM and TEM analysis have been realised in plane-view allowing counting of particles to be made on wide areas. The elemental compositions of thin films were examined by energy dispersive X-ray (EDX) analysis. Raman measurements were performed by Raman spectrometer at room temperature. Spectroscopic Ellipsometry (SE) measurements were recorded with a GES5 SOPRA made rotating polarizer SE, in the wavelength range 300 – 1500 nm with a step of 1 nm under incidence angle of 75°. Data acquisition and analysis were realized using the Winelli_II_Software (version 2.0.0.0). In this study, we investigate the optical properties of SiO_2 into PAM layer with SE in the wavelength range 300 - 1500 nm. SE allows accurate determination of film thickness (d), as well as refractive index (n) and extinction coefficient (k) as a function of wavelength and photon energy. Optical dispersion coefficients 'n' and 'k' were calculated in the case of SiO_2/PAM/TPP thin films structure using the BEMA model. The samples were excited by 488 nm of an Ar+-ion laser with a power of 20 Wcm^2. The spectral responses were collected to 250 Wcm^2 Jobin-Yvon monochromator equipped with a GaAs photomultiplier [26,27].

III. EXPERIMENTAL PROCEDURE

3.1. Fabrication of Porous Alumina Matrix(PAM)) Thin Films

Aluminum films (Al purity >99.999%) were deposited onto transparent polypropylene (TPP) leaf is very practical, easy to maneuver, low cost, does not absorb water, has a shiny appearance, and is temperature resistant to 160°C. Under vacuum ($3 \cdot 10^{-5}$ mbar) by thermal evaporation technique (tectra HC 3500). The deposited Al films thickness of ~550 nm was detected by using the monitor thickness tecta GmbH. The obtained Al thin films were anodized in 370% sulfuric acid (H2SO4) and 63% (H2O2) solution, under a constant DC-voltage of 7.3 V for 28 min at 10°C [28,29].

3.2. Energy Dispersive X–ray (EDX) Analysis

EDX technique was used to identify the elements composition of the SiO_2/PAM/TPP layers (Figure 1). As shown typical EDX spectrum presents the detected elements in the sample of SiO_2/PAM during 50 min of deposition time: Si, O and Al. EDX analysis shows that Si, O, and Al elements in the starting solution present in the SiO_2/PAM film, and the relative elemental composition are depicted in Figure 1. The average atomic percentage of Si, O and Al was 50.28%, 20.04% and 14.64%. The EDX result indicates that the samples are rich in several alkaline elements like Na, C, and Fe; all of them are usual components of the transparent polypropylene substrate. In Figure 2, after a mechanical and ionic thinning, we will do a TEM analysis to check the pores exist inside the PAM substrate, this image exhibit a large regularity of the PAM pores, whose the mean size of pores was obtained at about 55 nm. In Figure 3, typical EDX-mapping of the SiO2 deposition time during 50 min shows a quite homogeneous distribution of all the elements detected. Only Si, O and Al are showed. The Na, C, and Fe maps do not appear, which indicates that the elements are coming from the TPP substrate.

ISSN (Print) : 2320 – 3765

ISSN (Online): 2278 – 8875

International Journal of Advanced Research in Electrical, Electronics and Instrumentation Engineering

(An ISO 3297: 2007 Certified Organization)

Vol. 6, Issue 7, July 2017

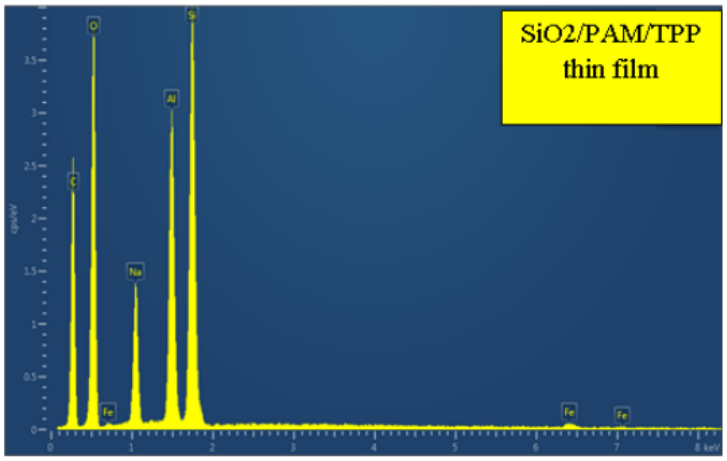

Figure 1: Typical EDX spectra of SiO2/PAM/TPP.

Sample	Element	Atomic%
SiO2/PAM/TPP thin film	O K	20.04
	Na K	10.75
	C K	4.05
	AL K	14.64
	Si K	50.28
	Fe K	0.23

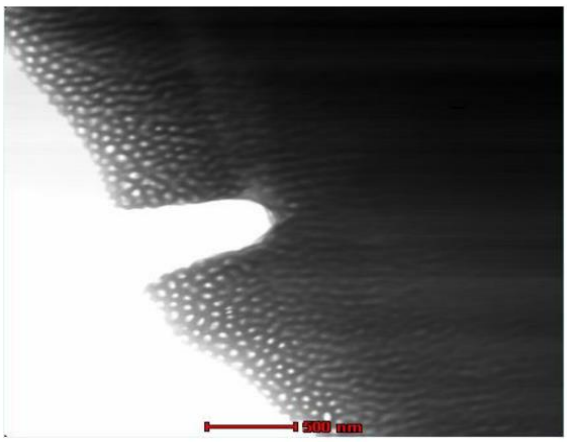

Figure 2: TEM of PAM thin film.

ISSN (Print) : 2320 – 3765

ISSN (Online): 2278 – 8875

International Journal of Advanced Research in Electrical, Electronics and Instrumentation Engineering

(An ISO 3297: 2007 Certified Organization)

Vol. 6, Issue 7, July 2017

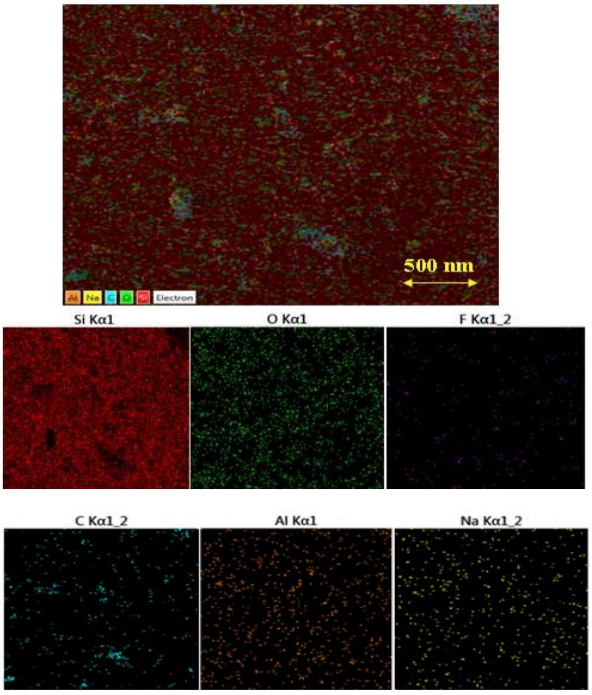

Figure 3: EDX-mapping of SiO2/PAM/TPP thin film during 50 min.

3.3. AFM Investigation

In order to contribute well to the improvement of the highly reflective layers intended to cover the reflecting parabola we used these types of substrates transparent polypropylene (TPP) which is very malleable, so one can expect a transportable reflectors. Figure 4 shows AFM images of layers of SiO2 at different deposition times on an alumina layer PAM using the PECVD technique. The AFM image shows an appearance of the wrinkles which disappear as a function of the deposition time varying from 20 to 60 minutes. An almost smooth surface is obtained for a deposition time of about 50 min after deposits. By exceeding 50 min, we notice the birth of crystals on the surface, SiO_2 grains preferentially give birth to the exuberant parts of the substrate. These grains see their sizes become larger and are distributed in an inhomogeneous manner on the surface; this type of morphology is shown on the last photo corresponding to a deposition time equal to 60 min.

ISSN (Print) : 2320 – 3765

ISSN (Online): 2278 – 8875

International Journal of Advanced Research in Electrical, Electronics and Instrumentation Engineering

(An ISO 3297: 2007 Certified Organization)

Vol. 6, Issue 7, July 2017

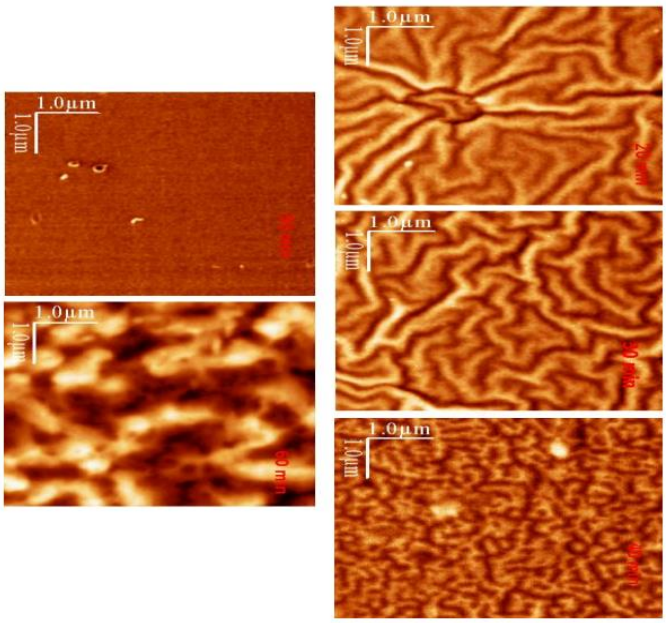

Figure 4: AFM micrograph of of SiO2/PAM/TPP thin film during 20, 30, 40, 50 and 60 min.

3.4. X-Ray Diffraction Analysis

Figure 5 shows XRD patterns of annealed SiO_2/PAM film at 550°C under nitrogen for differents depostion times (from 20 to 60 min). These samples show three diffraction peaks at 29.02°, 39.59°, 47.59°, 55°, 57.59° and 60° corresponding respectively to Si [111], Al [111], Si[220], Al_2O_3[202], Si[311] and Al[220] planes of cubic Si phase, with preferential orientation along Si[111]. As illustrated in Figure 5, the diffraction peak intensity of Si (111) plane was increased with the deposition time. The increase in peak intensities, as function of annealing duration, indicated a higher volumic phase transformation from the crystalline to amorphous Si. The mean crystallite size of SiO2 was calculated using Debey Scherrer's equation [30].

$$D = \frac{0.9\lambda}{\beta \cos\theta} \qquad (1)$$

Where D is the average crystallite size, λ is the X–ray wavelength, θ is the Bragg diffraction angle, and β is the adjusted FWHM. The obtained values of SiO2 size increased from 2.8 nm to 6.7 nm with the increase of deposition time from 120 min. Table 1 shows the variation of the obtained values indicated that the nanocrystallites size increased with the deposition time and that the largest nanocrystallites were obtained for the sample annealed at 150 min. The increase in the crystallite size was probably due to the decrease of void percentage and the diffused of small nanocrystals inside the pores of PAM layer during the deposition time. Therefore a diffusion in the wrinkles gives a layer almost amorphous, from where a surface almost smooth during the deposition time.

ISSN (Print) : 2320 – 3765

ISSN (Online): 2278 – 8875

International Journal of Advanced Research in Electrical, Electronics and Instrumentation Engineering

(An ISO 3297: 2007 Certified Organization)

Vol. 6, Issue 7, July 2017

	Raman spectroscopy				XRD patterns		
	Crystallite size D_{Raman} (nm)	Crystalline volume fraction X_{Raman} (%)	Residual Stress σ (MPa)	Crystallite size D_{XRD} (nm)	Microstrain (ε) × 10^{-3}	Dislocation density (ρ) × 1016 lines.m^{-2}	Number of crystallites per unit area (N) × 10^{18} m^{-2}
20	20.5	46.55	3717.3	28.8	46.25	19.73	20.73
30	28.2	52.28	2642.1	37.2	43.70	12.71	12.55
40	37.6	57.69	2441.5	39.9	37.04	8.02	6.44
50	19	62.05	342.2	22.6	29.5	5.55	4.42
60	73.3	82.73	1916.5	85.7	28.03	4.06	3.37

Table 1: Parameters obtained from XRD pattern and Raman spectroscopy for SiO2/PAM layers.

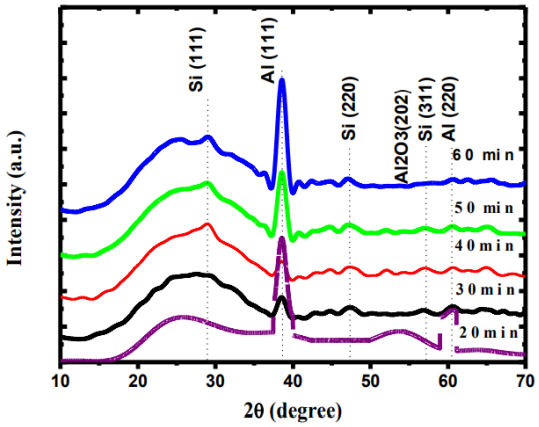

Figue 5: X-ray diffraction patterns of SiO2/PAM/TPP thin film during 20, 30, 40, 50 and 60 min.

3.5. Raman Analysis

In this part, we investigate the effect of the deposition time on the crystallinity of SiO2 /PAM layer by Raman spectroscopy. Figure 6 shows the Raman spectra of SiO2 /PAM films of deposition time from 20 min to 60 min. The peaks around 150 cm^{-1}, 300-380 cm^{-1}, and 480 cm^{-1} are related respectively to the crystalline, intermediate, and amorphous SiO2 phases [31]. The LO–TO peak shift provides data on the mean size of Si nanocrystals (D_{Raman}), the crystalline volume fraction (*X*Raman), and the stresses in the SiO2 /PAM thin films structure. The mean crystallite size of Si nanocrystals (D_{Raman}) was estimated using the following relation [32]:

$$D_{Raman} = 2\pi\sqrt{\frac{B}{\Delta\nu}} \qquad (2)$$

Where, ν is the peak shift for the nc-Si compared to the c-Si, and B = 2 cm^{-1} nm^2 [33].The crystalline volume fraction (XRaman)

ISSN (Print) : 2320 – 3765

ISSN (Online): 2278 – 8875

International Journal of Advanced Research in Electrical, Electronics and Instrumentation Engineering

(An ISO 3297: 2007 Certified Organization)

Vol. 6, Issue 7, July 2017

of Si thin film on the PAM layer was estimated from the following relation [10].

$$X = \frac{I_c + I_m}{I_c + I_m + I_a} \qquad (3)$$

Where *I*c is the integrated intensity of the SiO2 phase around 468 cm^{-1}, *I*m is the integrated intensity of the intermediate Si phase in the range 460-501 cm^{-1} and *I*a is the integrated intensity of the SiO2 phase at 302 cm^{-1}. Table 1 shows the change of the mean crystallite Si size and the crystalline volume fraction after deposition time. The obtained values display that the D_{Raman} and X_{Raman} have increased from 20.5 to 73.3nm and from 46.55 to 82.73%, respectively. The obtained values of average crystallite Si sizes are in good agreement with those calculated using XRD data.

The LO-TO phonon peak shift is the result of the various type of tensile stress, such as the growth of small Oxygen Si nanocrystals inside the PAM pores until reaching the external surface.

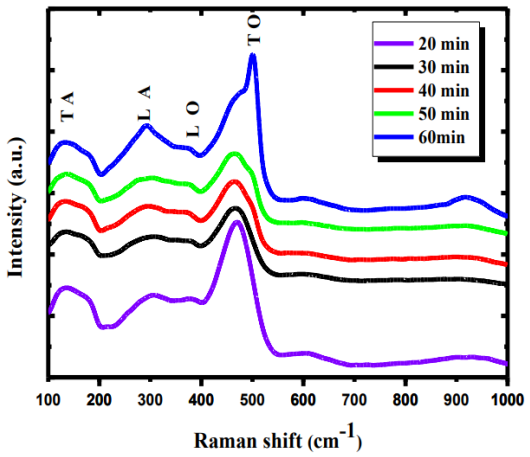

Figure 6: Raman spectra of SiO2/PAM/TPP thin film during 20, 30, 40, 50 and 60 min.

3.6. Modeling the Optical Constants of SiO2/PAM in Terms of Spectroscopic Ellipsometry

To study the effect of the microstructural characteristics on the optical properties of SiO2 deposited on PAM films, we focused on SE measurements. The purpose of this study is to determine the refractive index (n), the extinction coefficient (k), of the annealed SiO2/PAM thin films at 150°C for a different deposition time (20, 30, 40, 50, and 60 min).

The determination of the physical parameters (*n* , and *k*) depends on the adequate optical model to modulate *tan* (ψ) and *cos* ( ) experimental data. The constructed optical model of the multilayer structure is schematized in Figure 7. The two-component media of the model consist on the interface Al2O3/Al layer onto TPP substrate and three separate layers (layer 1, layer 2 and layer 3) with different thickness (d1, d2 and d3) and composed of SiO2-Al_2O_3 and void. The optical model is based on the additive contribution from each phase into the effective medium polarisability [34].

ISSN (Print) : 2320 – 3765

ISSN (Online): 2278 – 8875

International Journal of Advanced Research in Electrical, Electronics and Instrumentation Engineering

(An ISO 3297: 2007 Certified Organization)

Vol. 6, Issue 7, July 2017

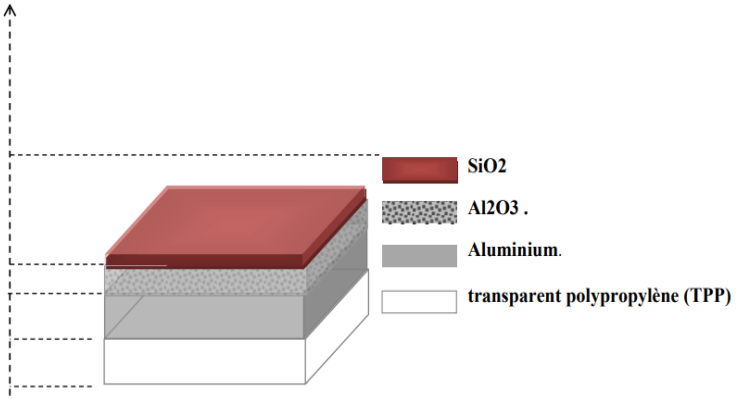

Figure 7: Ellipsometric model of the multilayer structure of SiO2/PAM.

From the SE analysis of unannealed and annealed SiO2/PAM films, the experimental and theoretical spectra of *tan* (ψ) and *cos* ( ) were obtained with a good concordance for all spectral range using BEMA model, as shown in Figure 8.

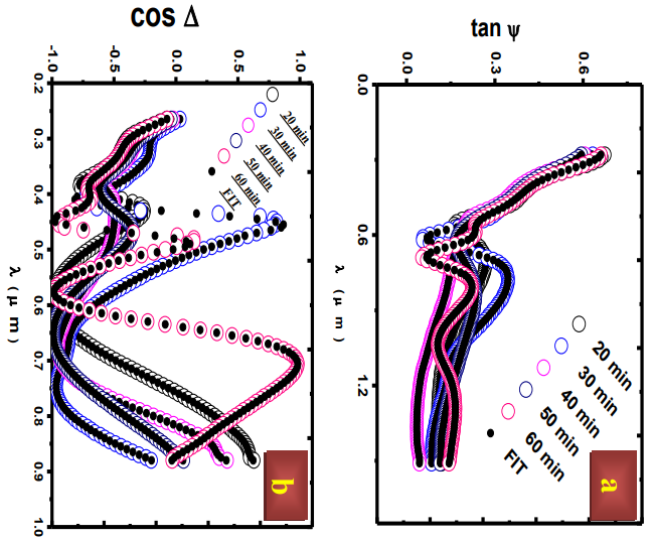

Figure 8: Experimentally measured (symbols) and fitted (red-lines) spectroscopic ellipsometry data of SiO2/PAM thin films at different deposition times.

The Bruggeman approximation for the multilayer structure is given by the following relation:

ISSN (Print) : 2320 – 3765

ISSN (Online): 2278 – 8875

International Journal of Advanced Research in Electrical, Electronics and Instrumentation Engineering

(An ISO 3297: 2007 Certified Organization)

Vol. 6, Issue 7, July 2017

$$f\frac{n(\text{sio}\,2)^2-(n)^2}{n(\text{sio}\,2)^2+2(n)^2}+Q\frac{1-(n)^2}{1+2(n)^2}=0 \qquad (4)$$

Where n(SiO2) is the refractive index of crystalline Si, n is the effective refractive index of mixed phase (amorphous+crystalline) of Si layer, Q is the volume fraction of the voids and f =1−Q is the volume fraction of SiO2 /PAM.

The goodness of fit of the optical model is obtained by using the following relation [35]:

$$RMSE=\sqrt{\frac{1}{2N-P-1}\sum_{j=1}^{N}\left[(\tan\psi_j^m-\tan\psi_j^s)+\left(\cos\Delta_j^m-\cos\Delta_j^s\right)^2\right]} \qquad (5)$$

Where N is the number of points, P is the number of parameters, m refers to measured spectra and s refers to simulated spectra.

The RMSE value of the annealed samples was found between 4.3×10^{-2} and 5.5×10^{-2}, which indicates a very good fit. The values of the fitted parameters for all the samples along with their RMSE values are illustrated in Table 2. As given in this table, the thickness of layer 1 (PAM) layer 2 (SiO2/ PAM) decreases with different time depostion due to diffusion of silica into the alumina part, and migration of core oxide to the outside, while the thickness of layer 3 increases with different time depostion. A similar trend is also shown in the voids percentage which can be influenced by the increase of deposition time, and the location of the crystals in PAM (Table 2).

	layer 1(d(nm))			layer 2(d(nm))			layer 3(d(nm))			
	d1	**SiO2 (%)**	***Q (%)***	**d2**	**SiO2 (%)**	***Q (%)***	**d3**	**SiO2 (%)**	***Q (%)***	**RMSE**
20	328.2	19.04	46.03	338.2	11.34	10.23	338.2	4.31	9.05	0.037
30	378.64	21.56	44.24	336.6	12.03	9.08	336.6	5.03	8.06	0.036
40	484.53	23.72	38.51	334.5	13.72	8.11	334.5	8.72	7.22	0.034
50	533.24	35.42	32.44	329.2	12.42	7.24	329.2	6.24	6.24	0.033
60	582.61	46.23	26.2	325.6	13.12	5.21	325.6	5.03	4.21	0.037

Table 2: Parameters extracted from the SE spectral-fitting for the SiO2/PAM layers. RMSE are reported in the same table.

The increase of the deposition time has an effect on differents parameters such as crystallites size, voids%, lattice strain, structural parameters,and layer structure.

Figure 9 exhibit respectively the spectra of extinction coefficient (k) and refractive index (n) resulting from the fitted parameters of the experimental data of *tan* (ψ) and *cos* ( ). We notice a pseudo-sinusoidal variation of refractive index, which is explained by a growth of the Si nano-crystals diffused in the wrinkles formed on the surface of PAM (Figure 10). The refractive index of the SiO2/PAM interlayers increased for deposition time to the amorphous (n2 = 2.8 at 550 nm for annealed sample at 550°C during 120 min) thin films. The value of n2 of a thin layer depends on the density of the material components and voids in the film structure. From Figure 11, we can also see that the extinction coefficient values found to decrease with the increase of deposition time.

ISSN (Print) : 2320 – 3765

ISSN (Online): 2278 – 8875

International Journal of Advanced Research in Electrical, Electronics and Instrumentation Engineering

(An ISO 3297: 2007 Certified Organization)

Vol. 6, Issue 7, July 2017

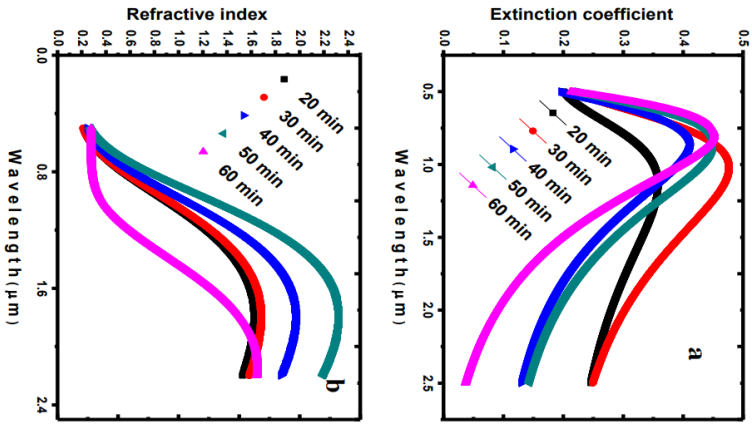

Figure 9: Extinction coefficient k (a) and refractive index n (b) of SiO2/PAM thin films at different deposition times.

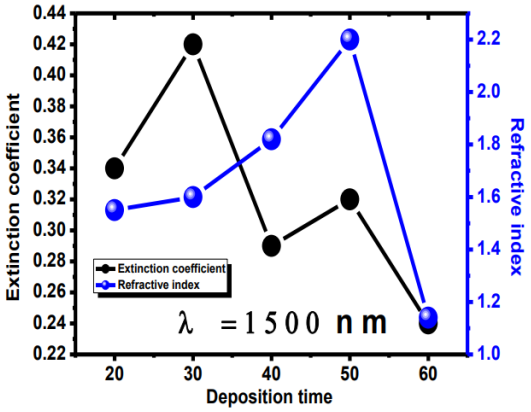

Figure 10: Refractive index and extinction coefficient versus deposition time of SiO2/PAM.

3.7. Photoluminescence (PL)

The PL measurements were carried out with an Ar^+ ion Laser source using an excitation 488 nm at room temperature for SiO2/PAM with different deposition times (20, 30, 40, 50, and 60 mn). As shown in Figure 11, a broad PL spectra of SiO2 on PAM templates were observed between ~2.2 eV towards ~1.3 eV corresponding to deposition times (20 mn, 30 mn, 40 mn, and 50 mn) respectively, Whereas for a time of deposits that is suitable for 60 min, it is observed that there is a return of displacement towards 1.4 eV to be explained by a simple growth of the nano spheres of SiO2 diffused on the surface. Compared by PL of PMA which is localized in 3.5 eV. The origin of this displacement is attributed to the quantum confinement of the SiO2 nanocrystals incorporated within PAM and the interface state effect between SiO2 and the PAM [36,37]. The origin of the decrease in PL intensity can be attributed to O_2 desorption groups incorporated inside the pores of PAM layer [11], resulting in the reduction of the dangling bonds and the structural defects such as dislocation density, micro-strains, and internal-stresses [38]. The deposition time promotes the decrease of the void percentage in the SiO2/PAM films, leading to get a more compact microstructure. Remarkable red-shifts of PL spectra were observed as a function of N2-annealing time. They resulted from the increase of Si nanocrystals size and the crystallinity improvement of SiO2 thin films into PAM template.

ISSN (Print) : 2320 – 3765

ISSN (Online): 2278 – 8875

International Journal of Advanced Research in Electrical, Electronics and Instrumentation Engineering

(An ISO 3297: 2007 Certified Organization)

Vol. 6, Issue 7, July 2017

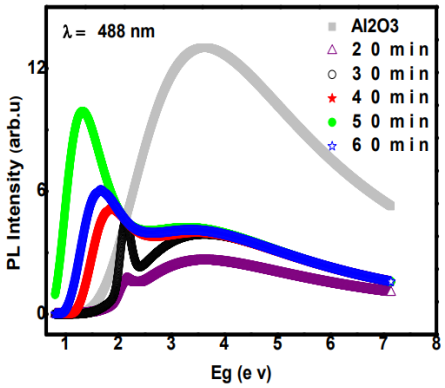

Figure 11: PL spectra of of SiO2/PAM thin films.

3.8. Reflectivity Analysis

An appearance of labyrinthine folds that gradually disappear by increasing the deposition time to reach a surface of almost zero roughness after 50 min of deposition. The extension of the deposition time to 60 min gives rise to aggregates of silicon on the surface of the samples whose dimension varies from 0.25 to 0.5 µm. Consequently the surface regains its rough character. The total reflectivity values of the SiO2/PAM/TPP samples increases from 78 to 99% for a λ = 1000nm when the deposition time increases from 20 to 50 min. Therefore a 50 min deposit gives us a 20% gain in reflectivity [39,40]. By slightly increasing the deposition time by 10 min, the surface regains its roughness and the reflectivity assumes a value of 80%. In other words, the reflectivity decreases by about 20% with respect to the maximum value of the 100% reflectivity. Figure 12 shows a model of a reflector which we have discerned by simple high-quality means, with a temperature reaching 150°C, which gives a reflectivity of 100% over all wavelengths.

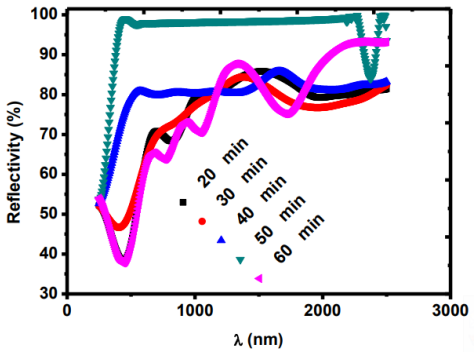

Figure 12: Total reflectivity of SiO2/PAM thin films at different deposition times and model of total reflector.

IV. CONCLUSION

In the present study, SiO2 were deposited into PAM layer by PECVD method and followed by different deposition time (20, 30, 40, 50, and 60 min) at 150°C. The deposition time was used to change the morphological, microstructural, and optical properties of the deposited SiO2 into PAM template. SEM micrographs exhibited the morphological modification of SiO2/PAM microstructure with the increase deposition time, resulting in the decrease in the voids percentage at the surface. From XRD study,

ISSN (Print) : 2320 – 3765

ISSN (Online): 2278 – 8875

International Journal of Advanced Research in Electrical, Electronics and Instrumentation Engineering

(An ISO 3297: 2007 Certified Organization)

Vol. 6, Issue 7, July 2017

we point out that the deposition time was a key factor, due to the decrease in the microstrain and the dislocation density of SiO2 in a PAM model leading to the improvement of an amorphous phase. Raman analyses show that crystallite Si sizes and the crystalline volume fraction have increased from 2.3 to 5.3 nm and from 62.86 to 81.73%, respectively. The obtained values of mean nc-Si sizes are in good agreement with those calculated using XRD data. The optical properties (*n*, *k*, and *E*g) of the SiO2/PAM nanostructure were evaluated from SE data. The different optical parameters were influenced by the change of crystalline volume fraction and SiO2 size with the variation of deposition time. From the PL measurements, we found that the PL bleu-shift is attributed to the increase of nanocrystallite size as a function of deposition time. The optical performance of solar reflectors depends on the structure and morphology of the surfaces and necessarily on the type of coating. We have developed new coatings based on SiO2/PAM, We were able to increase the total reflectivity to 100%. The increase of the peak intensity (LO–TO phonon) as a function of deposition time reveals the crystallinity and amorphous phase improvement of the film structure. In the present work, we highlighted that the remarkable change in peak position of LO–TO phonon is related to the increase in deposition time. This is probably due to the increase of the average size of Si nanocrystals. The obtained values of the mean.

V. REFRENCES

1. Ghrib M, Ouertani R, et al. Effect of annealing on photoluminescence and optical properties of porous anodic alumina films formed in sulfuric acid for solar energy applications. Appl Surf Sci 2012; 258: 4995–5000.
2. Valcheva E, Yordanov G, et al. Low temperature studies of the photoluminescence from colloidal CdSe nanocrystals prepared by the hot injection method in liquid paraffin. Colloids Surf A 2014; 461: 158–166.
3. Diguna LJ, Shen Q, High efficiency of CdSe quantum-dot-sensitized TiO2TiO2 inverse opal solar cells. Appl Phys Lett 2007; 91: 023116.
4. Chen J, Wu J, et al. Co-sensitized quantum dot solar cell based on ZnO nanowire. Appl Surf Sci 2010; 256: 7438–7441.
5. Kennedy C, Smilgys RV, Optical performance and durability of solar reflectors protected by an alumina coating, National Renew-able Energy aboratory NREL/TP-471-21413, No. SE612033, USA, 1996.
6. Ghrib M, Ouertani R, et al. Effect of annealing on photoluminescence and optical properties of porous anodic alumina films formed in sulfuric acid for solar energy applications. Applied Surface Science 2012; 258: 4995– 5000.
7. Sulka GD, Epniowski WJ, et al. Structural features of self-organized nanopore arrays formed by anodization of aluminum in oxalic acid at relatively high temperatures. Electrochem Acta 2009; 54:3683–3691.
8. Rousserie G, Sukhanova A, Formation of fluorescent polydopamine dots from hydroxyl radical-induced degradation of polydopamine nanoparticles. Crit Rev Oncol Hemat 2010; 74: 1–15.
9. Valcheva E, Yordanov G, et al. Low temperature studies of the photoluminescence from colloidal CdSe nanocrystals prepared by the hot injection method in liquid paraffin. Colloids Surf A 2014; 461: 158–166.
10. Diguna LJ, Shen Q, et al. Fibrous CdS/CdSe quantum dot co-sensitized solar cells based on ordered TiO2 nanotube arrays. Appl Phys Lett. 2007; 91: 023116.
11. Tonucci RJ, Justus BL, et al. Ngnochannel array glass. Science 1992; 258: 783.
12. Whitney TW, Jiang JS, et al. Fabrication and magnetic properties of arrays of metallic nanowires. Front matter. Science 1993; 261: 1361.
13. Laatar F, Hassen M, et al. Correlation between microstructural and optical properties of silicon thin films grown onto porous alumina by plasma–enhanced CVD method. J Alloy Comp 2016; 658: 337.

ISSN (Print) : 2320 – 3765

ISSN (Online): 2278 – 8875

International Journal of Advanced Research in Electrical, Electronics and Instrumentation Engineering

(An ISO 3297: 2007 Certified Organization)

Vol. 6, Issue 7, July 2017

14. Laatar F, Hassen M, et al. Effect of air-annealing on the morphological, microstructural and optical properties of CdSe NCs grown into porous anodic alumina template. Superlattices Microst 2015; 83: 575–587.
15. Liao CL, Wu MT, et al. Preparation of RF-sputtered lithium cobalt oxide nanorods by using porous anodic alumina (PAA) template. J Alloy Comp 2006; 414: 302-309.
16. Dabboussi S, Elhouichet H, et al. Excitation and emission processes of Tb3+ in porous anodic alumina. Appl Surf Sci 2009; 255: 4255-4258.
17. Gyanan, Jayakrishna K, Synthesis of luminescent CdTe nanorods on anodized aluminum oxide template and their utility in divalent heavy metal ion sensing. Soft Nanosci Lett 2014; 4: 69-74.
18. Mondal SP, Dhar A, et al. Optical properties of CdS nanowires prepared by dc electrochemical deposition in porous alumina template. Mater Sci Semicond Process 2007; 10: 185-193.
19. Ghrib M, Gaidi M, et al. Morphological and optical properties changes in nanocrystalline Si (nc-Si) deposited on porous aluminum nanostructures by plasma enhanced chemical vapor deposition for Solar energy applications. Appl Surf Sci 2011; 257: 9129.
20. Hoyer P, Baba N, et al. Small quantum-sized CdS particles assembled to form a regularly nanostructured porous film. Appl Phys Lett 1995; 66: 2700.
21. Dongsheng Xu, Yajie Xu, et al. Preparation and characterization of CdS nanowire arrays by dc electrodeposit in porous anodic aluminum oxide templates. Chem Phys Lett 2000; 325: 340.
22. Zhao WB, Zhu J, et al. Photochemical synthesis of CdSe and PbSe nanowire arrays on a porous aluminum oxide template. Scr Mater 2004; 50: 1169.
23. Koch F, Petrova-Koch V, et al. Quantum confinement effects on the dielectric constant of porous silicon. Mater Res Soc Symp Proc 1992; 283: 197–202.
24. Averboukh B, Huber R, et al. Luminescence studies of a Si/SiO_2 superlattice. J Appl Phys 2002; 92: 3564–3568.
25. Bessais B, Ben Younes O, et al. Morphological changes in porous silicon nanostructures: non-conventional photoluminescence shifts and correlation with optical absorption. J Lumin 2000; 90: 101.
26. Hadjisavvas G, Kelires PC, Structure and energetics of Si nanocrystals embedded in a−SiO_2 Phys Rev Lett 2004; 93: 226104.
27. Godefroo S, Hanyne M, et al. Red spectral shift and enhanced quantum efficiency in phonon-free photoluminescence from silicon nanocrystals. Nat. Nanotechnol 2008; 3: 174–178.
28. Cullis AG, Canham LT, Visible light emission due to quantum size effects in highly porous crystalline silicon. Nature 1991; 353: 335–338.
29. John GC, Singh VA, Theory of the photoluminescence spectra of porous silicon. Phys Rev 1994; 50: 5329.
30. Ali G, Ahmad M, Novel structure formation at the bottom surface of porous anodic alumina fabricated by single step anodization process. Micron 2010; 41: 560–564.
31. Cullity BD, Elements of X-ray diffraction (2nd edn.). Addition-Weasley, London, 1978.
32. Funde AM, Bakr NA, Hybrid Si microwire and planar solar cells: passivation and characterization. Sol Energy Mater Sol Cells 2008; 92: 1217–1223.
33. Gajovic A, Gracin D, Correlating Raman-spectroscopy and high-resolution transmission-electron-microscopy studies of amorphous/nanocrystalline multilayered silicon thin films. Thin Solid Films 2009; 517: 5453–5458.

ISSN (Print) : 2320 – 3765

ISSN (Online): 2278 – 8875

International Journal of Advanced Research in Electrical, Electronics and Instrumentation Engineering

(An ISO 3297: 2007 Certified Organization)

Vol. 6, Issue 7, July 2017

34. He Y, Yin C, et al. Electronic conductivity of hydrogenated nanocrystalline silicon films. J Appl Phys 1994; 75: 797.
35. Schnyder B, Kötz R, et al. Spectroscopic ellipsometry and XPS studies of anodic aluminum oxide formation in sulfuric acid. J Electroanal Chem 1992; 339: 167.
36. Petrik P, Fried M, et al. Ellipsometric characterization of nanocrystals in porous silicon. J Appl Surf Sci 2006; 253: 200–203.sd
37. Ali AM, UV irradiation and H2 passivation processes to classify and distinguish the origin of luminescence from thin film of nc-Si deposited by PECVD technique. J Alloy Comp 2015; 623: 89–95.
38. Tong GB, Muhamad MR, et al. Photoluminescence and structural properties of silicon nanostructures grown by layer-by-layer deposition. Opt Mater 2012; 34: 1282–1288.
39. Farva U, Park C, Colloidal synthesis and air-annealing of CdSe nanorods for the applications in hybrid bulk hetero-junction solar cells. Mater Lett 2010; 64: 1415.
40. Fend T, Jorgensen G, et al. Applicability of highly reflectiv aluminum coil for solar concentrators. Sol Energy 2000; 68: 361–370.